Plant Biotechnology Journal
Open Access

Plant Biotechnology Journal (2025) **23**, pp. 3864–3878 doi: 10.1111/pbi.70165

Editing *cis*-elements of *OsPHO1;2* improved phosphate transport and yield in rice

Kanika Maurya[1], Balaji Mani[1], Bhagat Singh[1], Ujjwal Sirohi[1], Aime Jaskolowski[2], Sandeep Sharma[3], Harsha Vardhan Tatiparthi[4], Satendra Kumar Mangrauthia[4], Renu Pandey[3], Yves Poirier[2] and Jitender Giri[1,*]

[1]*National Institute of Plant Genome Research, New Delhi, India*
[2]*Department of Plant Molecular Biology, University of Lausanne, Lausanne, Switzerland*
[3]*Mineral Nutrition Laboratory, Division of Plant Physiology, ICAR-Indian Agricultural Research Institute, New Delhi, India*
[4]*Indian Institute of Rice Research, Hyderabad, Andhra Pradesh, India*

Received 26 November 2024;
revised 4 April 2025;
accepted 12 May 2025.
**Correspondence* (Tel 91-1126735227; fax 91-11-26741658; email jitender@nipgr.ac.in)

Summary

Increasing grain yield is the primary goal of crop improvement, which is globally affected by the low availability of soil phosphate (Pi). Overexpressing Pi transporters to enhance Pi uptake often results in Pi toxicity and growth retardation. Despite advances in genetic engineering, targeting the *cis*-regulatory motifs of Pi transporters remains underexplored for understanding plant mechanisms and improving Pi status. Here, we demonstrate that the excision of the transcription inhibitor motif from the promoter of the Pi transporter *OsPHO1;2* enhances its expression and increases root-to-shoot Pi transport, leading to improved grain yield. Through *in silico* and DNA-protein interaction studies, we show the role of the OsWRKY6 transcription factor in negatively regulating *OsPHO1;2* expression by binding to the *cis*-regulatory element (*W-box*) present in its promoter. The *oswrky6* knockout lines exhibit higher *OsPHO1;2* expression and improved shoot Pi levels. Furthermore, we engineered the *OsPHO1;2* promoter to precisely remove the *W-box* and enhance *OsPHO1;2* expression. Phenotypic and physiological evaluations at the vegetative stage indicate that *OsPHO1;2* promoter-edited (*OsPHO1;2:PE*) lines have increased shoot length, plant biomass and greater root-to-shoot Pi export under both low and normal P conditions. Notably, the ^{33}P uptake assay reveals that *OsPHO1;2:PE* lines display enhanced root Pi uptake, supported by higher expression of root-associated Pi transporters (*OsPHTs*). An extensive agronomic assessment shows that *OsPHO1;2:PE* lines achieve increased seed and panicle numbers, thereby raising yield without affecting seed quality. Our findings provide valuable insights into the potential of promoter editing to improve Pi use and enhance crop yield.

Keywords: *PHOSPHATE1*, phosphate transport, CRISPR/Cas9, promoter editing, yield enhancement.

Introduction

Phosphorus (P) is an essential macronutrient for growth, development and yield, particularly in crop plants. It is critical in physiological and metabolic processes such as photosynthesis, respiration and cellular signalling (Yang *et al.*, 2024). Plants primarily obtain soluble inorganic orthophosphate (Pi) from the soil. However, Pi in soils can quickly precipitate with other minerals (iron and aluminium), forming non-soluble complexes, while microbes convert it into organic compounds (López-Arredondo *et al.*, 2014). Due to the limited availability of soil Pi, crops often suffer from Pi deficiency, which negatively impacts plant growth and productivity globally, leading agriculture to rely heavily on Pi fertilizers to achieve high productivity (Elser *et al.*, 2017; Jiao *et al.*, 2012). Nonetheless, due to finite P reserves, high costs and environmental risks, such as eutrophication, reliance solely on Pi fertilizers is problematic and unsustainable (Campos-Soriano *et al.*, 2020; Lun *et al.*, 2018; MacDonald *et al.*, 2011). Therefore, it is essential to comprehend the mechanisms underlying plant responses to Pi starvation and leverage them for crop improvement aimed at efficient P use.

Among various adaptive responses at the morphological, biochemical and physiological levels, fine-tuning the expression of phosphate transporters in response to low Pi availability is critical for plants (Poirier *et al.*, 2022). Root P acquisition from the rhizosphere is an energy-requiring process executed by the epidermal or cortical cells expressing H^+/Pi co-transporters. In rice, at least thirteen members belonging to the PHT1 family have been identified expressing in the root and involved in Pi acquisition (Paszkowski *et al.*, 2002).

After Pi is absorbed by the roots, it is translocated to the shoot by another class of Pi transporter expressed in xylem parenchyma cells, known as PHOSPHATE1 (PHO1), which belongs to the SYG1/PHO81/XPR1-ERD1/XPR1/SYG1 (SPX-EXS) family (Poirier *et al.*, 1991; Stefanovic *et al.*, 2007; Wang *et al.*, 2004). Among the three members of the rice PHO1 family (OsPHO1;1, OsPHO1;2 and OsPHO1;3), OsPHO1;2 is primarily responsible for root-to-shoot Pi export (Secco *et al.*, 2010). OsPHO1;2 is a plasma membrane-localized transporter expressed in the root, young panicle, hulls and developing seeds (Ma *et al.*, 2021). *ospho1;2* mutants exhibit impaired Pi transfer, resulting in excessive phosphorus accumulation in the roots, deficiency in the shoots and underdeveloped grains (Che *et al.*, 2020; Ko

et al., 2024; Secco *et al*., 2010). Recently, Ma *et al*. (2024) demonstrated that OsPHO1;2 functions in regulating leaf photosynthesis, with its mutation leading to decreased electron transport activity and CO_2 assimilation (Ma *et al*., 2024). The homologues of PHO1 in other crops include SiPHO1 in tomatoes, and members of CaPHO1 in chickpeas play a major role in root-shoot Pi translocation (Mani *et al*., 2024; Zhao *et al*., 2019). PHO1 proteins contain the SPX domain at the N-terminus, transmembrane α-helices in the middle, and the EXS domain at the C-terminus. Studies have demonstrated that SPX proteins function as sensors for cellular Pi status by binding inositol pyrophosphate (PP-InsPs) molecules and regulating the phosphate starvation response (PHR) (Nagpal *et al*., 2024; Luo *et al*., 2024). Furthermore, the EXS domain of AtPHO1 may assist in the uncoupling mechanism of Pi starvation and growth retardation (Rouached *et al*., 2011; Wege *et al*., 2016). This evidence underscores the additional role of PHO1 in plant P signalling, which remains poorly understood.

Rice feeds more than half the world's population, yet nearly 50 per cent of rice-growing regions encounter Pi scarcity (Navea *et al*., 2024). Plants that overexpress PHTs or have mutations in PHT inhibitors can potentially boost phosphate acquisition efficiency (PAE). However, increases in Pi uptake frequently lead to Pi toxicity and hinder growth (Gu *et al*., 2016). For instance, overexpressing *OsPHT1;2*, *OsPHT1;8* or *OsPHT1;9* improves Pi uptake and transport but also results in Pi toxicity, reducing biomass and yield, particularly under Pi-sufficient conditions (Jia *et al*., 2011; Liu *et al*., 2010; Wang *et al*., 2014). Optimizing PHT1 expression may help prevent Pi overaccumulation and improve P starvation tolerance. Editing *cis*-regulatory elements in gene promoters presents a promising strategy for regulating gene expression and developing desired traits while minimizing negative effects.

Details on WRKY domain transcription factors (TFs) mediated regulation of PHT transporters are emerging. These TFs contain the conserved domain WRKYGQK and bind to *W-box* or *W-box like cis*-element motif 'TTGACC/T' in the promoter of various genes, including *PHTs*. WRKY TFs are involved in diverse processes influencing growth and plant signalling (Jiang *et al*., 2017; Ulker and Somssich, 2004). For instance, OsWRKY75 maintains tolerance to Pi starvation by regulating various OsPHTs (Devaiah *et al*., 2007). In Arabidopsis, *AtPHO1* is negatively regulated by AtWRKY6 and AtWRKY42. The double mutant *atwrky6atwrky42* exhibits increased expression of *AtPHO1* and a greater Pi transport to shoot (Chen *et al*., 2009; Su *et al*., 2015; Ye *et al*., 2018). Despite this, our current knowledge of the transcriptional regulation of rice *PHO1;2* remains elusive.

Here, we uncovered the molecular mechanism underlying the negative regulation of *OsPHO1;2* expression and presented an appealing strategy for enhancing its expression by modifying the *cis*-regulatory motif in its promoter. We report that the promoter of *OsPHO1;2* contains a *W-box* element recognized by OsWRKY6, which suppresses *OsPHO1;2* expression and shoot Pi transfer. We applied CRISPR/Cas9-based promoter editing using two gRNAs to excise the *W-box* site to increase *OsPHO1;2* expression while minimizing the pleiotropic effects potentially associated with *oswrky6* knockouts. Our results further revealed that *W-box* removal increases *OsPHO1;2* expression, promotes shoot Pi transfer, enhances Pi uptake and improves overall plant P status without compromising seed quality. Moreover, the *W-box* removal strategy increases panicle number and ultimately boosts grain yield by up to 26%. These findings highlight the potential of using a promoter editing strategy to enhance crop productivity.

Results

OSWRKY6 binds to *OsPHO1;2* promoter and regulates its expression negatively

In Arabidopsis, *PHO1* is transcriptionally regulated by WRKYs (Chen *et al*., 2009; Ye *et al*., 2018). However, the regulation of *PHO1* in rice remains unclear. Using the online PlantCare tool, we identified several *cis*-regulatory motifs, including ABRE, G-box, MYB and MYC binding sites in the ~1.4 kb promoter of *OsPHO1;2* (Lescot *et al*., 2002). Additionally, we noted a potential *W-box* motif at −1280 bp, prompting an investigation into its role in transcriptional regulation.

In rice, there are about 100 members of the WRKY TF family (Rushton *et al*., 2010). Gene co-expression analysis conducted using the public gene co-expression database RiceFREND (https://ricefrend.dna.affrc.go.jp/) to explore which WRKY TF potentially regulates *OsPHO1;2* expression suggests that only one WRKY TF family member, OsWRKY6, co-expresses with *OsPHO1;2* (Table S1). In addition, the WRKY domain of OsWRKY6 shares 54% and 75.4% sequence identity and similarity, respectively (http://imed.med.ucm.es/cgi-bin/sias/) to the AtWRKY6 protein, which has been studied for regulating *AtPHO1* expression (Chen *et al*., 2009; Ye *et al*., 2018). Moreover, phylogenetic analysis of the WRKY TFs in Arabidopsis and rice has revealed that OsWRKY6 is one of the closest homologues to AtWRKY6 (Wu *et al*., 2005). Hence, all these data suggest that OsWRKY6 may play a role in regulating *OsPHO1;2* expression.

Transient expression of an eYFP-WRKY6 fusion in *N. benthamiana* demonstrated localization to the nucleus (Figure S1). To explore the expression pattern of *OsWRKY6*, we analysed its transcript levels in different developmental tissues. *OsWRKY6* is expressed significantly higher in seeds, followed by the roots and stem base (Figure 1a). This expression pattern was further validated by histological β-glucuronidase (GUS) analysis in various tissues of *OsWRKY6-promoter:GUS* reporter lines (Figure 1b). Interestingly, the transverse section of the roots showed GUS expression specifically in the stelar region, coinciding with the expression of *OsPHO1;2* (Figure 1b(ii)) (Ma *et al*., 2021).

We next investigated whether OsWRKY6 can bind directly to the *W-box* in the *OsPHO1;2* promoter (*OsPHO1;2p*) using an electrophoretic mobility shift assay (EMSA). Our results indicated that OsWRKY6 binds to the *W-box* site in *OsPHO1;2p*. However, the mutation of the *W-box* attenuates OsWRKY6's binding to *OsPHO1p* (Figure 1c). To understand how OsWRKY6 regulates *the* expression of *OsPHO1;2*, we generated *oswrky6* mutants using the CRISPR/Cas9 tool and selected lines based on the sequencing data of the target site. The selected *oswrky6* mutants carry a 1 bp deletion that results in a null mutant (Figure S2). The transcript levels of *OsWRKY6* in these mutants were lower compared to the WT (Figure S3). We transiently expressed the *OsPHO1;2p:GUS* construct in the rice roots of wild type (WT) and *oswrky6* knockout plants. As shown in Figure 1d, *oswrky6* knockout roots exhibited a strong GUS signal compared to the WT, as visualized by GUS staining of the whole roots and their cross-sections, which was further confirmed by quantifying GUS activity (Figure 1d,e; Figure S4). These findings suggest that OsWRKY6 negatively regulates

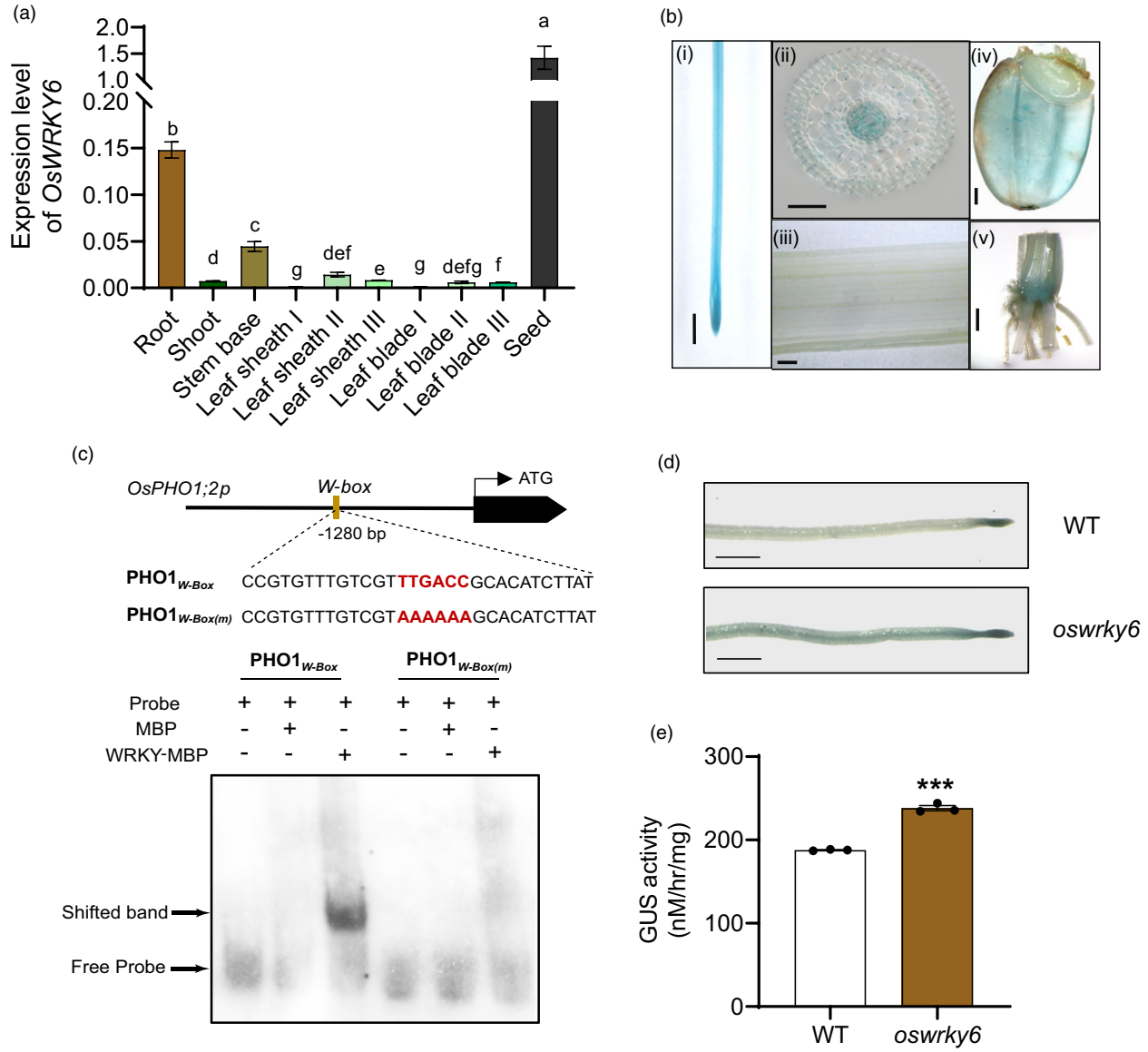

Figure 1 *OsWRKY6* co-expresses with *OsPHO1;2* and regulates its expression. (a) The expression pattern of *OsWRKY6* in different rice tissues was determined by RT-qPCR. *Ubiquitin5* was used as an endogenous control. Data represent means ± SE (n = 3, each replicate contains a pool of 5 seedlings). Significant differences between different tissues are indicated with different letters ($P < 0.05$, one-way ANOVA). (b) Tissue-specific localization in ((i) root, (ii) transverse section of root, (iii) shoot, (iv) seed, (v) stem base) of *OsWRKY6* using GUS reporter lines driven by *OsWRKY6* promoter. Scale bar: i, iii–v: 1000 μm, ii: 50 μm. (c) Electrophoretic mobility shift assay (EMSA) showing OsWRKY6 binding to *W-box* ($PHO1_{W\text{-}Box}$) in *OsPHO1;2* promoter *in vitro*. The *W-box* mutated promoter sequence ($PHO1_{W\text{-}Box(m)}$), in which the TTGACC mutated to AAAAAA, does not show the mobility shift with OsWRKY6. Also, empty vector (MBP) shows no shift with probes. (d, e) Transient expression assay in rice seedlings showing repressor activity of OsWRKY6 on *OsPHO1;2* expression. (d) Images of 3-day-old rice seedlings (wild type (WT) and *oswrky6*) transformed with *OsPHO1;2p*:GUS construct followed by GUS staining. Scale bar: 1000 μm. (e) Quantitative measurement of GUS activity in rice roots. Data represent means ± SE (n = 3, each replicate contains a pool of 5 seedlings). Each dot represents one biological replicate. Significant changes were determined using the Student's t-test. *** indicates a significant difference from WT at P-value ≤0.001.

OsPHO1;2 expression by directly interacting with the *W-box* in the *OsPHO1;2* promoter.

Knocking out *OsWRKY6* increases *OsPHO1;2* expression in roots

Next, to examine the effect of OsWRKY6 knockout on the regulation of *OsPHO1;2* expression and to validate our *in vitro* data, we analysed the *OsPHO1;2* expression in the roots of these *oswrky6* mutants. Remarkably, the *oswrky6* mutants exhibited higher levels of *OsPHO1;2* transcripts in their roots compared to the WT (Figure 2a). Consequently, the increased *OsPHO1;2* expression was linked to greater Pi accumulation in the shoots of *oswrky6* mutants than in WT (Figure 2b). The *oswrky6* knockouts showed up to approximately 27% and 21% increases in shoot Pi under low and normal P conditions, respectively. However, phenotypic analysis revealed that *oswrky6* mutants grew similarly

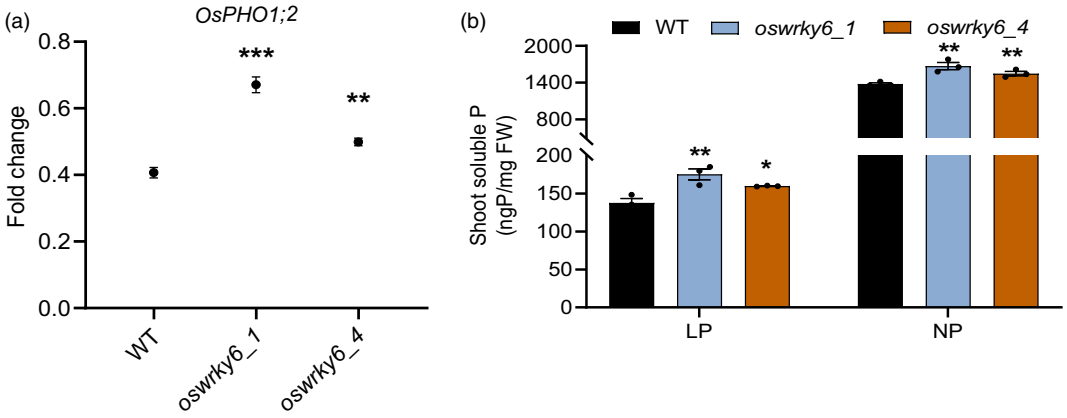

Figure 2 *oswrky6* knockout lines show enhanced *OsPHO1;2* expression with improved shoot Pi concentration. (a) Expression level of *OsPHO1;2* in root tissue of 9-day-old seedlings of wild type (WT) and *oswrky6* mutants. Expression level was calculated as fold change ($2^{-\Delta CT}$). *Ubiquitin5* was used as an endogenous control. Data represent means ± SE (n = 4, each replicate contains a pool of 5 seedlings). (b) Soluble P estimation in shoots of 21-day-old seedlings of WT and *oswrky6* mutants grown under low (10 μM NaH_2PO_4, LP) and normal P (320 μM NaH_2PO_4, NP) conditions. Data represent means ± SE (n = 3, each replicate contains a pool of 5 seedlings). Each dot represents one biological replicate. Significant changes were determined using the Student's t-test. *, ** and *** indicate significant difference from control (WT) at P-value ≤0.05, ≤0.01 and ≤0.001, respectively.

to WT and did not display any significant differences in shoot length and plant biomass under various Pi conditions (Figure S5).

These results indicate that OsWRKY6 reduces Pi transfer to the shoot by negatively regulating OsPHO1;2 activity. Mutation in OsWRKY6 improves Pi transfer to the shoot, intriguingly, with no discernible changes in plant growth.

Precise removal of OsWRKY6 binding site from *OsPHO1;2*'s promoter (*OsPHO1;2p*) contributes to enhanced *OsPHO1;2* expression and improves shoot Pi

Based on the results above, shoot P levels can be enhanced by overexpressing *OsPHO1;2* or suppressing *OsWRKY6*. Targeted promoter editing is an intriguing alternative to fine-tune gene expression and create new traits without generating loss-of-function mutants or introducing transgenes. In this regard, we aimed to increase the expression of *OsPHO1;2* by removing the *W-box* from its promoter using CRISPR/Cas9.

Two gRNAs flanking the *W-box* region (located at the −1280 bp position) in *OsPHO1;2p* were designed, and stable transgenic rice plants were generated (Figure 3a). The target region was examined for editing using fragment-specific PCR, and we obtained gene-edited plants featuring a deletion of approximately 30 bp in the *OsPHO1;2* promoter (Figure S6). In the T_2 generation, progenies were also screened for the absence of the Cas9 transgene to select Cas9-free biallelic edited lines (Figure S7). Two randomly chosen Cas9-free progenies, *OsPHO1;2:PE5* and *OsPHO1;2PE8*, were selected and characterized to identify mutations using Sanger sequencing. Sequencing results revealed deletions of 35 bp and 33 bp in *OsPHO1;2:PE5* and *OsPHO1;2PE8*, respectively, with both deletions occurring in the *W-box* region of the *OsPHO1*;2p (Figure 3b). Furthermore, we studied potential off-target mutations using the CRISPR GE tool (http://skl.scau.edu.cn/) and detected 13 and 12 putative off-targets for gRNA1 and gRNA2, respectively. Most off-targets were found in intergenic and intronic regions with equal or more than 3 mismatches in the seed region (Table S2). The top five off-targets showing the highest off-target scores were selected and screened. Upon screening a pool of 10–15 plants, a much lower off-target score was obtained for both *OsPHO1;2:PE* lines (Table S3). Additionally, the distribution of off-target mutations occurred in non-coding regions, suggesting high specificity of the designed gRNAs for *W-box* excision.

Next, we studied the impact of *OsPHO1;2p* editing on *OsPHO1;2* gene expression by performing RT-qPCR on the root tissues of *OsPHO1;2:PE* lines (Figure 3c). Our results showed that *OsPHO1;2* expression was significantly elevated in both *OsPHO1;2:PE* lines, suggesting that the removal of the *W-box* positively regulates *OsPHO1;2* expression. Furthermore, the ^{33}P transfer rate was examined in the *OsPHO1;2:PE* lines, as OsPHO1;2 in rice serves as a major Pi exporter for root–shoot translocation (Secco *et al.*, 2010). We observed a 32% increase in root–shoot ^{33}P transfer rate in *OsPHO1;2:PE* lines compared to the WT (Figure 3d). Additionally, the increased expression of *OsPHO1;2* led to higher Pi levels in shoot tissue, with substantial increases of up to 48% and 41% in the shoots of *OsPHO1;2:PE* lines under low and normal P conditions, respectively (Figure 3e). These findings were also accompanied by a significantly greater total shoot P level in the *OsPHO1;2:PE* lines (Figure S8a).

Subsequently, we monitored the growth performance of *OsPHO1;2:PE* lines at the vegetative stage under different P concentrations (Figure 3f). Compared to wild-type (WT), *OsPHO1;2:PE* lines exhibited more than 11.5% and 9% increases in shoot length under low and normal P conditions, respectively (Figure 3g). A similar trend was observed in plant biomass and shoot dry weight, where *OsPHO1;2:PE* lines showed an increase of up to 21% compared to WT (Figure 3h; Figure S8b).

Therefore, we concluded that at the early vegetative stage, the removal of the OsWRKY6 binding site, specifically the *W-box* (TTGACC/T), increases *OsPHO1;2* expression, leading to greater Pi transfer to the shoot and enhanced plant growth.

OsPHO1;2:PE lines show higher root P accumulation with induction in root associated PHT expression

Interestingly, when we examined the root phenotype, *OsPHO1;2:PE* lines exhibited shorter roots compared to WT (Figure 4a). In contrast, the number of roots in *OsPHO1;2:PE* lines increased by approximately 22–55% under both low and normal P conditions (Figure 4b). This prompted us to investigate the Pi status of the

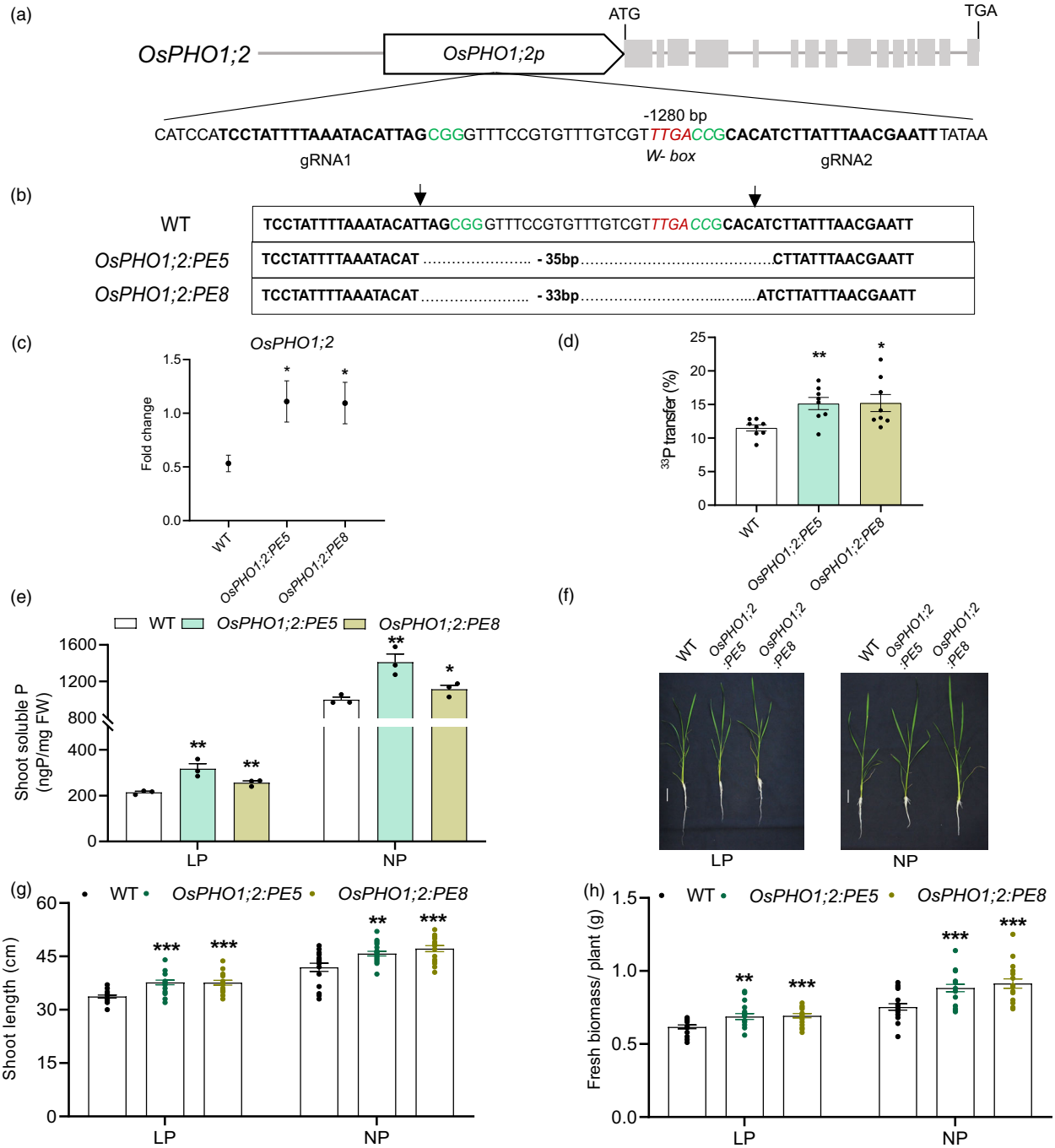

Figure 3 Promoter editing of *OsPHO1;2* enhances *OsPHO1;2* expression with improved shoot Pi transport and plant growth. (a) Schematic illustration of *OsPHO1;2* gene and its promoter (*OsPHO1;2p*). The introns and exons are represented by grey-colour line and rectangle boxes, respectively. The translation initiation codon (ATG) and termination codon (TGA) are shown. The *W-box* sequence (TTGACC) in *OsPHO1;2p* is represented by a red colour italicized sequence. The gRNA sequences (gRNA1 and gRNA2) are in bold. (b) Sanger sequencing analysis of *OsPHO1;2:PE* plants. The CRISPR/Cas9 mediated deletion of *OsPHO1;2p* sequence is indicated in base pairs. gRNA sequences are in bold, nucleotides marked in green represent PAM; arrow denotes putative Cas9 cut site (3 bp upstream to PAM); *W-box* is represented by red coloured and italicized sequence. For Sanger sequencing, the DNA fragment spanning the target sites was amplified using primers spanning gRNAs, followed by sequencing. (c) The expression level of *OsPHO1;2* in root tissue of 9-day-old seedlings of wild type (WT) and *OsPHO1;2:PE* lines. Expression level was calculated as fold change ($2^{-\Delta CT}$). *Ubiquitin5* was used as an endogenous control. Data represent means ± SE (n = 4, each replicate contains a pool of 5 seedlings). (d) ^{33}P transfer rate from root to shoot in 9-day-old seedlings of WT and *OsPHO1;2:PE* lines. Data represent means ± SE (n = 8). (e) Soluble P estimation in shoot tissues of 21-day-old seedlings of WT and *OsPHO1;2:PE* lines grown under low (10 μM NaH_2PO_4, LP) and normal P (320 μM NaH_2PO_4, NP) conditions. Data represent means ± SE (n = 3). (f) Phenotypic analysis, (g) shoot length and (h) plant biomass of 21-day-old seedlings of WT and *OsPHO1;2:PE* lines grown under LP and NP conditions. Data represent means ± SE (n = 15–20). Each dot represents one biological replicate. Scale bar: 5 cm. Significant changes were determined by the Student's *t*-test. *, ** and *** indicate significant difference from control (WT) at *P*-value ≤0.05, ≤0.01 and ≤0.001, respectively.

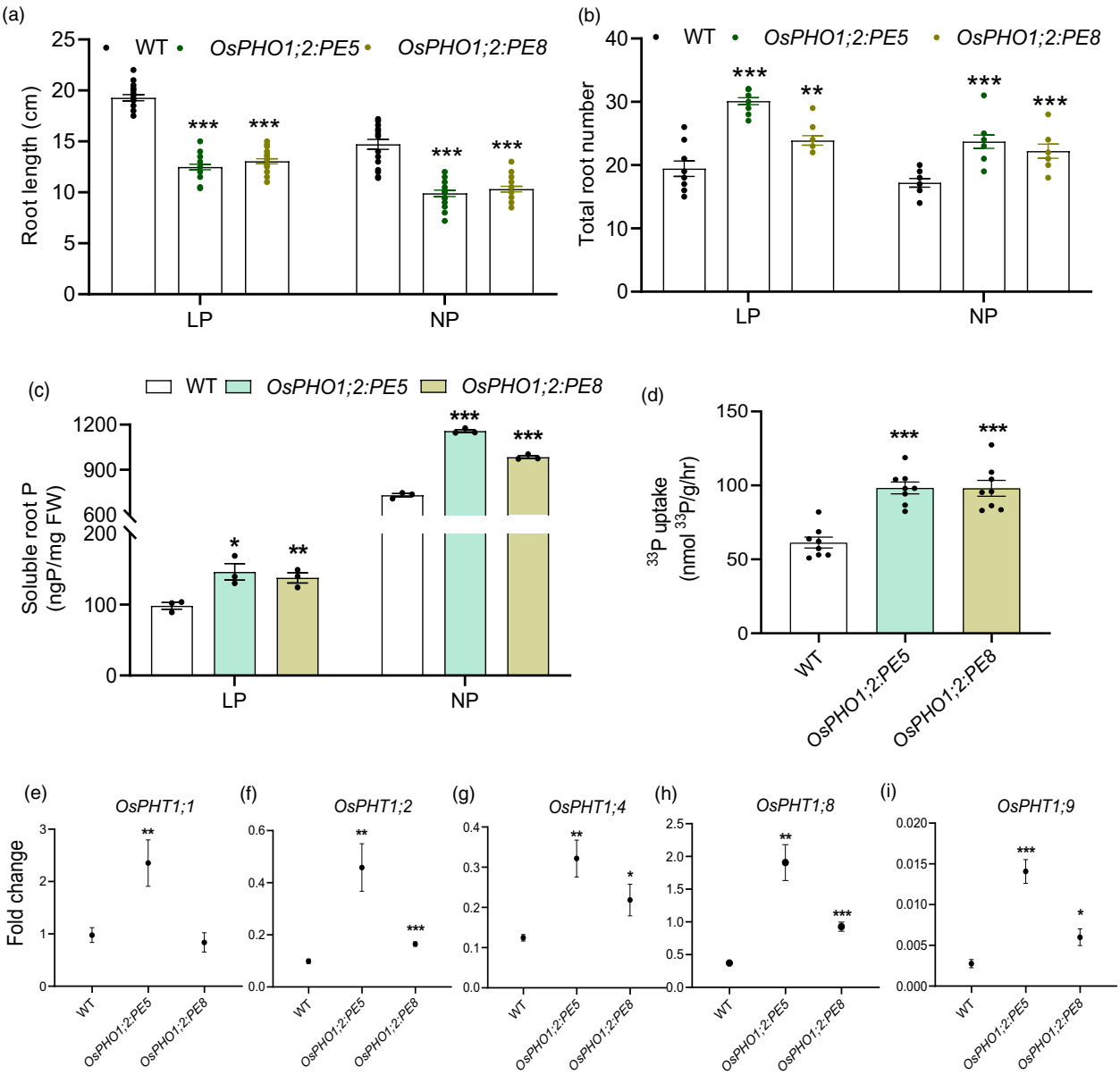

Figure 4 Promoter editing of *OsPHO1;2* increased Pi uptake. (a) Root length (n = 15–20) and (b) total number of roots (n = 8–10) measurement in 21-day-old seedlings of wild type (WT) and *OsPHO1;2:PE* lines grown under low (10 μM NaH_2PO_4, LP) and normal P (320 μM NaH_2PO_4, NP) conditions. (c) Root soluble P in 21-day-old seedlings of WT and *OsPHO1;2:PE* lines grown under LP and NP conditions. Data represent means ± SE (n = 3, each replicate contains a pool of 5 seedlings). (d) ^{33}P uptake rate in 9-day-old seedlings of WT and *OsPHO1;2:PE* lines. ^{33}P uptake rate represents the amount of ^{33}P absorbed by the roots from the external solution per mg of root fresh weight. Data represent means ± SE (n = 8). (e–i) Expression of phosphate transporters (*OsPHTs*); (e) *OsPHT1;1*, (f) *OsPHT1;2*, (g) *OsPHT1;4*, (h) *OsPHT1;8* and (i) *OsPHT1;9* in root tissue of 9-day-old seedlings of WT and *OsPHO1;2:PE* lines. Expression level was calculated as fold change ($2^{-\Delta CT}$). *Ubiquitin5* was used as an endogenous control. Data represent means ± SE (n = 4, each replicate contains a pool of 5 seedlings). Each dot represents one biological replicate. Significant changes were determined by the Student's t-test. *, ** and *** indicate significant differences from control (WT) at P-value ≤0.05, ≤0.01 and ≤0.001, respectively.

roots. Compared to WT, the roots of *OsPHO1;2:PE* lines accumulated over 40% and over 34% higher Pi under low and normal P conditions, respectively (Figure 4c). Likewise, we observed significantly greater total P in the roots of *OsPHO1;2:PE* lines (Figure S9a). Furthermore, we noted an enhanced ^{33}P uptake of up to 60% by the roots of *OsPHO1;2:PE* lines compared to WT, suggesting that the higher Pi levels in roots are related to increased Pi uptake mediated by root Pi transporters (Figure 4d). To confirm this possibility, we analysed the expression of root-associated *OsPHTs* in *OsPHO1;2:PE* lines and detected a significant increase in the expression of *OsPHT1;1*, *OsPHT1;4*, *OsPHT1;8* and *OsPHT1;9* (Figure 4e–i). Notably, a significant rise in the expression of the low-affinity Pi transporter *OsPHT1;2* was observed. With this data, we calculated root efficiency in *OsPHO1;2:PE* lines, which represents the total amount of P accumulated within the plant for the same root surface area. Our observations showed that root efficiency is enhanced in *OsPHO1;2:PE* lines. Thus, the increased expression of *OsPHO1;2* resulted in the heightened expression of root *OsPHTs*, leading to elevated P levels in roots of *W-box* edited lines, indicating improved root efficiency in *OsPHO1;2:PE* lines (Figure S9b).

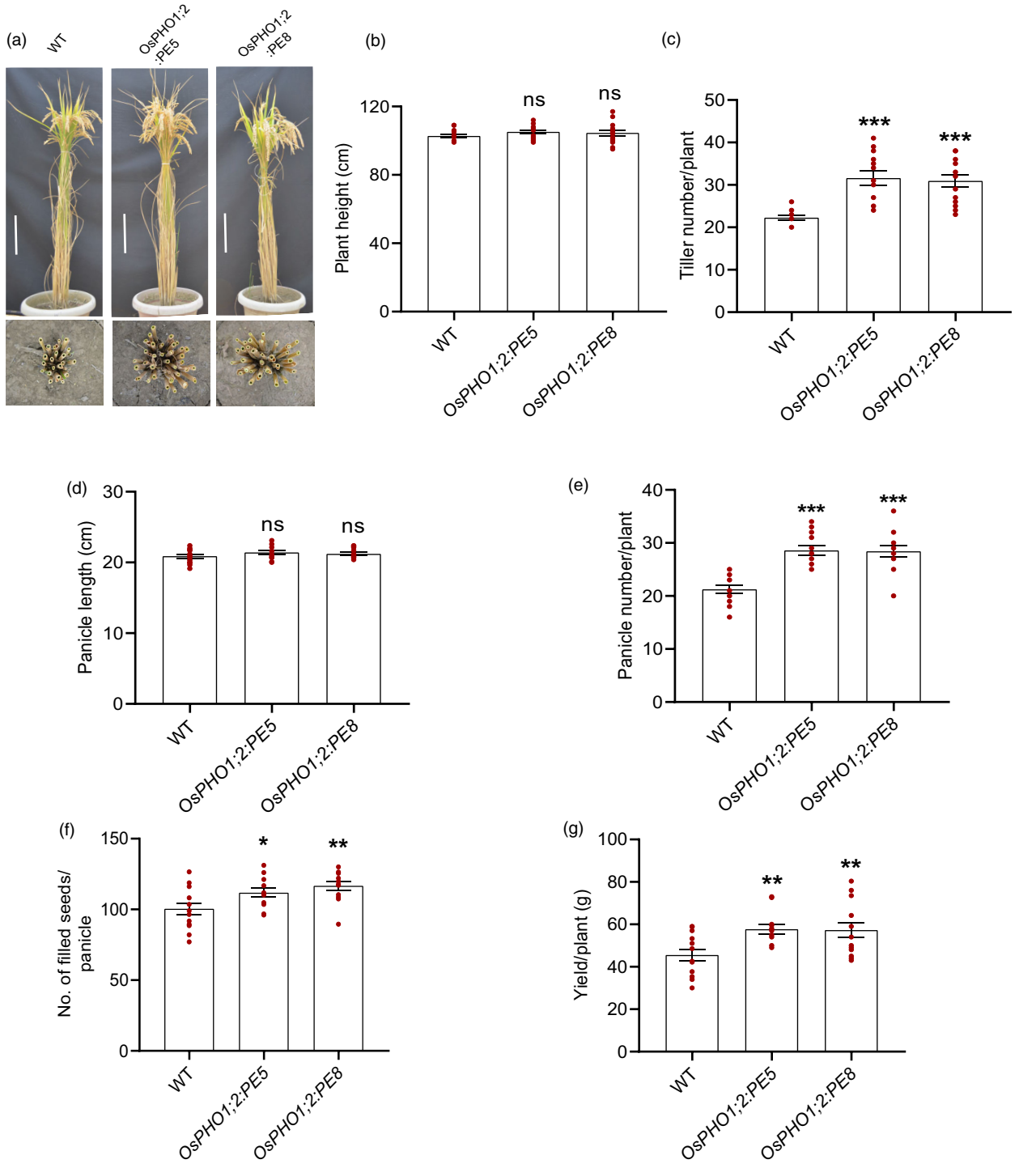

Figure 5 Promoter editing of *OsPHO1;2* improves yield-related traits in rice (Year 2023). Agronomic performance of WT and *OsPHO1;2:PE* lines at mature stage: (a) Gross morphology and tillers of WT and *OsPHO1;2:PE* lines at mature stage, (b) plant height, (c) tiller number, (d) panicle length, (e) panicle number/ plant, (f) number of filled seeds/ panicle and (g) yield/ plant. Data represent means ± SE (n = 12–15). Each dot represents one biological replicate. Significant changes were determined by the Student's t-test. ns indicate no significant difference. *, ** and *** indicate significant differences from control (WT) at P-value ≤0.05, ≤0.01 and ≤0.001, respectively. Scale bar: 20 cm.

W-box removal of *OsPHO1;2* promoter improves panicle number and plant yield

Next, we evaluated the growth performance of *OsPHO1;2:PE* lines in soil-filled pots with normal P supply. To this end, we phenotyped the *OsPHO1;2:PE* lines in 2023 and 2024. During the 2023 season, the plant height, leaf length, leaf width, flag leaf length, flag leaf width and panicle length of *OsPHO1;2:PE* lines showed no significant difference compared to WT (Figure 5a,b,d; Figure S10a–d). However, reproductive traits such as tiller number

and panicle number per plant in *OsPHO1;2:PE* lines significantly increased by 26–45% compared to WT (Figure 5c,e). A closer examination of the panicles revealed that the branch number per panicle and branch length remained unchanged, while a few panicle branches showed a marginal increase in seeds per branch in *OsPHO1;2:PE* lines (Figure S10e–g). Remarkably, the number of filled seeds per panicle improved in *OsPHO1;2:PE* lines compared to WT, leading to a higher seed yield (Figure 5f,g). A similar trend of an increased number of tillers, panicles and yield was observed in the 2024 season (Figure S11). Additionally, we assessed the performance of *OsPHO1;2:PE* lines in soil fertilized with lower phosphorus levels. Compared to WT, plant height, flag leaf width and panicle length were reduced in *OsPHO1;2:PE* lines; however, these plants exhibited a greater number of panicles and improved seed yield (Figure S12).

Our results indicate that removing the *W-box* from the *OsPHO1;2* promoter increases panicle number, which leads to a higher grain yield in *OsPHO1;2:PE* lines under both low and normal P supply.

OsPHO1;2:PE seeds have reduced P content with no compromise in quality

Apart from panicle number, seed number and total plant yield, grain quality is a critical factor in rice for human consumption (Hori and Sun, 2022; Zhou *et al*., 2020). Since *OsPHO1;2:PE* lines showed higher yield because of increased panicle number per plant, we examined seed quality using parameters such as seed size, length and width in WT and *OsPHO1;2:PE* lines. Our results showed *OsPHO1;2:PE* seed dimensions were comparable to WT, and no significant variation was observed (Figure 6a–d). The primary component of rice endosperm is starch granules, which act as carbohydrate storage and ultimately determine the cooking quality (Yu *et al*., 2009; Zhu *et al*., 2023). Rice seeds were cut in half and observed under the scanning electron microscope to observe starch granule morphology. Most of the starch granules were polygonal in shape and tightly packed in seeds of both WT and *OsPHO1;2:PE* lines with no visible differences (Figure 6e). This result was further supported by the iodine staining of seeds and the quantification of starch and amylose content (Figure 6f, Figure S13).

Recent reports have shown that the expression of *OsPHO1;2* influences seed development through a maternal effect by regulating Pi content in the endosperm, leading to *ospho1;2* mutants exhibiting low starch content and shrunken seeds (Ko *et al*., 2024; Ma *et al*., 2021). We observed that *OsPHO1;2:PE* lines accumulate slightly less total seed P content than WT (Figure 6g). Additionally, the grain physiological phosphate use efficiency (PPUE) is increased in *OsPHO1;2:PE* lines, suggesting that the seed P content of *OsPHO1;2:PE* lines contributes to producing a greater number of seeds and ultimately a higher yield (Figure S14). Furthermore, since Pi and Fe are finely tuned to regulate plant growth (Lay-Pruitt *et al*., 2022), we profiled Fe content in seeds and found that changes in seed Pi concentration do not impact Fe content (Figure S15). Phytic acid is the principal storage form of P in seeds and an antinutrient for human consumption (Bloot *et al*., 2021; Nissar *et al*., 2017). Due to its chelating properties, high phytic acid levels in seeds can lead to indigestion and other health-related issues. Therefore, we examined the phytic acid content of *OsPHO1;2:PE* lines and found no noticeable variation in the amount of phytic acid compared to WT (Figure 6h). Additionally, no differences were observed in the 1000-seed weight or germination percentage in *OsPHO1;2:PE* lines compared to WT seeds (Figure 6i,j).

Collectively, we demonstrate that *OsPHO1;2PE* lines produce completely normal seeds regarding size and quality. Additionally, these promoter-edited lines do not exhibit any reproductive defects.

Discussion

Over the last century, grain production has heavily relied on phosphate fertilizers, which have boosted global crop yields. By 2050, as the world population approaches 10 billion, demand for P fertilizer will exceed 22–27 Tg P yr^{-1}. Agricultural P use efficiency (PUE) must rise to 80% to meet food demands (Zou *et al*., 2022). Among cereals, rice exhibits low PUE, necessitating more fertilizer for crop production in countries such as India (Zou *et al*., 2022). As a major importer of P fertilizers, India needs to enhance its PUE through changes in agricultural practices (Langhans *et al*., 2022). Furthermore, global overapplication of P fertilizers, which exceeds optimal plant needs by 30–40%, causes nutrient runoff and leads to algal blooms and hypoxia (Lun *et al*., 2018; McDowell *et al*., 2024). Thus, effective crop production requires better fertilizer management and a deeper understanding of plant phosphate transport. Gene editing presents a groundbreaking method for advancing plant biology and addressing various agricultural issues (Ahmar *et al*., 2020). Our study utilized CRISPR/Cas9 to modify the *cis*-regulatory region of the phosphate transporter OsPHO1;2, thereby enhancing P transport and yield under varying P conditions.

WRKY transcription factors (TFs) are key players in plant signalling pathways related to biotic and abiotic stresses (Wang *et al*., 2023; Wani *et al*., 2021). Our initial sequence analysis indicated that OsWRKY6 shares a high sequence similarity with the *AtPHO1* inhibitor, AtWRKY6 and co-expresses with *OsPHO1;2* in roots (Figure 1). Interestingly, by binding to the *W-box* site in the *OsPHO1;2* promoter, OsWRKY6 suppresses *OsPHO1;2* expression, which is further validated by increased *OsPHO1;2* expression in roots and enhanced shoot Pi accumulation in *oswrky6* knockout lines (Figures 1, 2). All these findings confirm the role of OsWRKY6 in negatively regulating *OsPHO1;2* expression. However, these results contradict the previously reported function of OsWRKY6 as an activator of *OsPR10a* and *OsPR1* genes related to defence processes (Choi *et al*., 2015). Hence, these observations suggest a dual role for OsWRKY6 in activating *OsPR10a* while suppressing *OsPHO1;2* expression by binding to the *W-box* in their promoters. A similar dual function has also been reported for AtWRKY42, which acts as an activator and suppressor for *AtPHT1;1* and *AtPHO1* expression, respectively (Chen *et al*., 2009; Su *et al*., 2015).

Agronomically essential cereal crops such as rice, wheat and barley exhibit very low Pi fertilizer use efficiency (~10–20%), leading to a significant amount of fertilizers being precipitated and drained into water bodies, which causes eutrophication (Ojeda-Rivera *et al*., 2022). Thus, enhancing phosphorus acquisition efficiency (PAE) from soil benefits both plants and the environment. The PHT1 transporters expressed in roots primarily facilitate Pi uptake in plants (Mudge *et al*., 2002; Nussaume *et al*., 2011), and boosting root-associated PHT activity maximizes the utilization of available Pi in the soil. Ma *et al*. (2021) highlight that *OsPHO1;2* overexpression improves plant yield; however, they did not discuss its effect on *PHT1* expression and root morphology. Here, in addition to increased root-to-shoot Pi

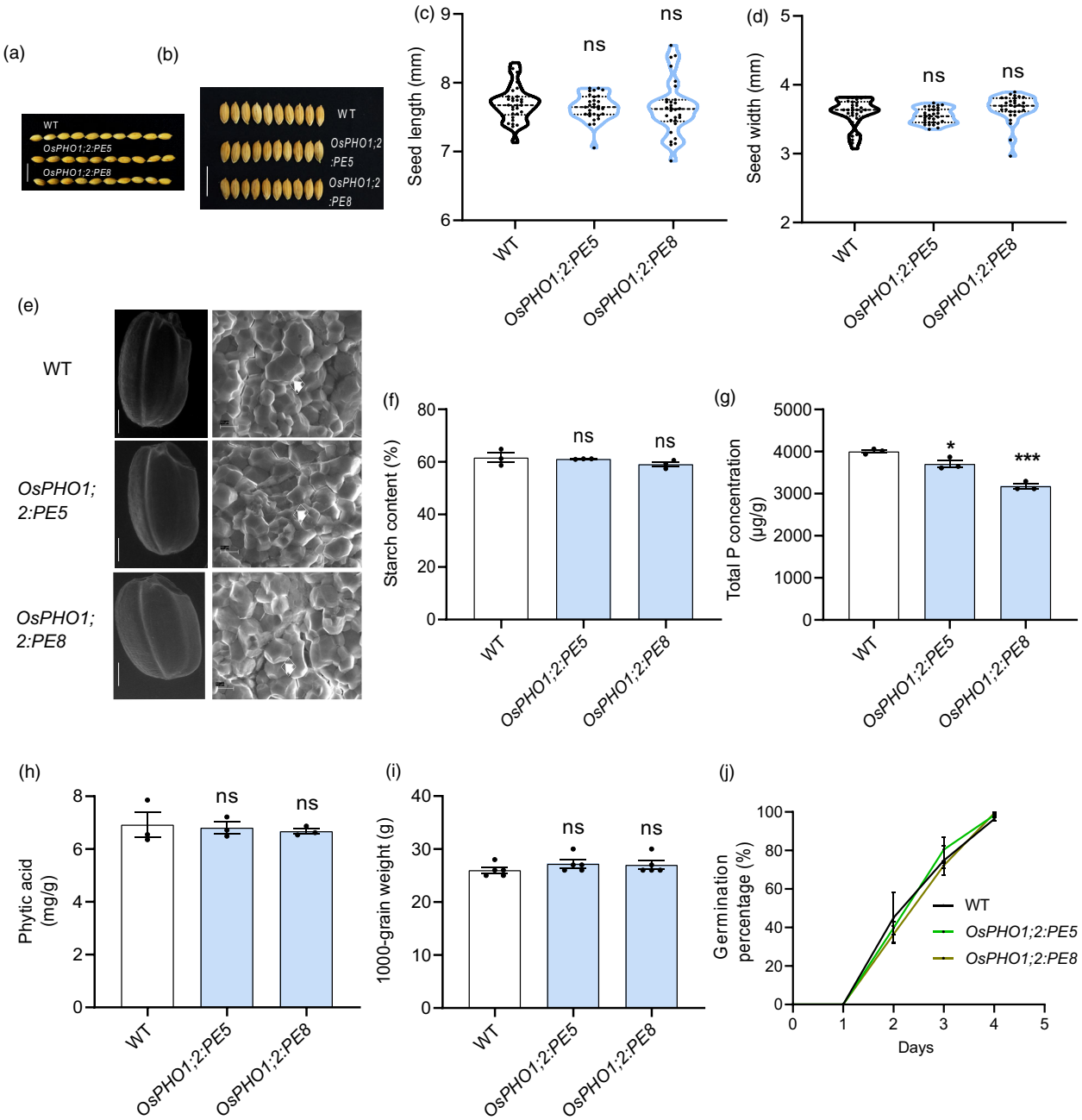

Figure 6 *OsPHO1;2:PE* lines show no penalty in seed quality. (a) Seed length and (b) seed width phenotype of mature seeds of wild type (WT) and *OsPHO1;2:PE* lines. Scale bar: 1 cm. (c) Seed length and (d) seed width measurement of mature seeds of WT and *OsPHO1;2:PE* lines (n = 30 seeds). (e) Scanning electron microscopic images of whole seed (scale bar: 30 mm) and middle cross-sections (scale bar: 10 µm) of brown seeds of WT and *OsPHO1;2:PE* lines. Arrow indicates packaging of starch granules. Measurement of (f) starch content, (g) total P concentration and (h) phytic acid in brown seeds of WT and *OsPHO1;2:PE* lines. Data represent means ± SE (n = 3). (i) 1000 grain weight (n = 5) and (j) Germination percentage of WT and *OsPHO1;2:PE* lines (n = 3, 30 plants in each replicate). Data represent means ± SE. Each dot represents one biological replicate. Significant changes were determined by the Student's *t*-test. ns indicate no significant difference. * and *** indicate significant difference from control (WT) at *P*-value ≤0.05 and ≤0.001, respectively.

transport, *OsPHO1;2:PE* lines display enhanced root P content (Figure 4). We further revealed that the increase in root P occurs through the induction of *OsPHT1*'s expression in *OsPHO1;2:PE* roots, leading to greater Pi uptake from the media (Figure 4). Additionally, modifications in root architecture, such as a higher root number and reduced root growth, were noted in *OsPHO1;2:PE* lines (Figure 4). This aligns with previous findings where Pi accumulation in the roots of *OsPHT1;8* overexpressing plants resulted in reduced root growth (Jia *et al*., 2011). We believe that the reduced root growth coupled with higher P accumulation observed in *OsPHO1;2:PE* lines might be a trade-off mechanism for maintaining slower root growth to redirect carbon flow toward improving aerial growth. Furthermore, containing SPX and EXS domains, PHO1 functions as both a Pi sensing protein and a transporter (Wang *et al*., 2021). Therefore, we propose that *OsPHO1;2*-driven increased Pi transport from root to shoot

creates a positive driving force in roots to absorb more Pi from the external environment, thereby activating root-associated *PHT1*s and enhancing Pi uptake. However, further research is necessary to fully understand how root-associated genes or *OsPHTs* are directly regulated by OsPHO1;2.

Both *oswrky6* mutants and *OsPHO1;2:PE* lines exhibit enhanced *OsPHO1;2* expression and improved shoot Pi accumulation compared to WT (Figures 2 and 3). However, the effect of increased *OsPHO1;2* expression on growth patterns is not evident in *oswrky6* mutants when compared to *OsPHO1;2:PE* lines (Figure S5). Our findings provide the following explanations: (i) A transcription factor (TF) can have multiple target genes. For example, AtWRKY42 targets both *AtPHO1* and *AtPHT1;1* (Su *et al*., 2015). Consequently, OsWRKY6 may regulate various targets related to stress and development (Choi *et al*., 2015). This results in knocking out *OsWRKY6* only restoring average plant growth despite high P content; and (ii) multiple TFs may target the same gene (Dergilev *et al*., 2021). For instance, both AtWRKY6 and AtWRKY42 suppress *AtPHO1* expression. Thus, various WRKY repressors may preferentially interact with the *OsPHO1;2 W-box* site alongside OsWRKY6 and the repressive activity of these TFs is inhibiting growth in *oswrky6* mutants. Therefore, our genome editing approach to delete *cis*-regulatory elements from the *OsPHO1;2* promoter reduces the potential for multiple repressors to bind to the *W-box* and quantitatively adjusts gene expression to enhance grain yield.

In plants, gene promoter sequences primarily define gene expression and modulate various aspects of adaptive developmental plasticity (Brázda *et al*., 2021). For instance, variations in the *OsSGR* promoter sequence among different indica rice subspecies result in distinct senescence patterns (Shin *et al*., 2020). Additionally, natural variations in the *ZmICE1* promoter exhibit different responses to cold treatment (Jiang *et al*., 2022). Besides using gene editing to unravel the function of a gene and create desired traits, promoter editing is emerging as a powerful tool across various crops to enhance qualitative traits, increase stress tolerance and boost yield (Shi *et al*., 2023; Tang and Zhang, 2023). A complete knockout of several genes, including transcription factors (TFs), could lead to unexpected and lethal consequences due to their multifunctionality within the plant system. Furthermore, due to the functional redundancy of TFs, eliminating the activity of one does not guarantee that the target site will be affected or yield the desired phenotype (Venezia and Creasey Krainer, 2021; Wu and Lai, 2015). Conversely, fine gene regulation through the removal of TF binding sites via promoter editing offers the advantage of adjusting gene intensity without disrupting their roles in other cellular processes, resulting in predictable phenotypes and a balanced trade-off. Moreover, modifying promoter elements expands genetic resources for synthetic biology and crop enhancement by introducing new germplasm and unique alleles (Tang and Zhang, 2023; Wu *et al*., 2024). A recent study by Wang *et al*. (2024) showed that deleting the repressor motif in the promoter of the *NF-YC4* gene increases *NF-YC4* expression and enhances protein content. In our study, we implemented a strategy of modifying the promoter using a multiple gRNA approach to create a small deletion in the promoter of *OsPHO1;2*. We demonstrated that the *OsPHO1;2:PE* lines exhibit enhanced *OsPHO1;2* expression in roots, along with increased shoot phosphate accumulation and improved plant growth (Figure 3). The results also indicate that *OsPHO1;2:PE* lines enhance yield-related traits such as panicle number and overall yield without compromising grain quality (Figures 5 and 6). Similar improvements in grain yield were reported when targeting the promoters of GS3 and D18 using CRISPR/Cas12a to increase grain size and panicle number, respectively (Shi *et al*., 2023; Zhou *et al*., 2023). Our strategy is preferable to earlier methods of overexpressing Pi transporters, which induce Pi toxicity and hinder growth retardation while increasing P in plants (Jia *et al*., 2011; Wang *et al*., 2014). Thus, we demonstrated that our promoter editing method for the Pi transporter gene improves plant performance in soils treated with normal and limited P fertilizer (Figure 5; Figures S11 and S12).

In summary, phosphate deficiency remains a crucial factor impacting crop productivity. Various potential strategies could be explored to enhance P acquisition and utilization for crop improvement. For instance, overexpressing *PSTOL1* and phosphate transporters can boost P uptake and low P tolerance (Gamuyao *et al*., 2012; Zhang *et al*., 2014). Additionally, bioengineered P-solubilizing bacteria possess the capability to release Pi from organic substances. Transgenic plants expressing the bacterial gene *ptxD* (phosphite oxidoreductase) could metabolize phosphite (López-Arredondo and Herrera-Estrella, 2012). However, these approaches introduce transgenes, which are not socially acceptable for crop plants. Our discovery of CRISPR/Cas9-based promoter modification demonstrates a forward-thinking approach for editing transcription repressor sites in the promoter of *OsPHO1;2* to improve Pi transport and yield (Figure 7). The transgene-free promoter-edited plants could serve as a valuable resource for commercializing rice varieties that yield better under low P input soils.

Experimental procedures

Dehusked rice (*Oryza sativa* L. ssp. *japonica*) cultivar Nipponbare (WT) seeds were surface sterilized with 0.1% $HgCl_2$ and pre-germinated on half-strength Murashige and Skoog (MS) media. After four days, germinated seedlings were transferred to hydroponics Yoshida media supplemented with low P (10 μM NaH_2PO_4, LP) and normal P (320 μM NaH_2PO_4, NP) concentrations as described (Mehra *et al*., 2019; Singh *et al*., 2015). The growth assessment experiments were conducted for 21 days in a growth chamber with a day/night temperature of 30 °C/24 °C, 16 h (light)/8 h (dark) photoperiod (400–450 μmol photons m^{-2} s^{-1}) and a relative humidity of 60%.

For gene expression analysis using RT-qPCR, seeds were inoculated in 1/4th MS media in hydroponics for 9 days. Root tissues were harvested and snap-frozen in liquid nitrogen. The samples were stored at −80 °C until RNA extraction.

To investigate the seed germination percentage, surface sterilized seeds were allowed to germinate on water-soaked germination paper. The percentage was calculated at intervals of 1–4 days.

gRNA designing, vector construction and rice transformation

To raise promoter-GUS reporter plants of *OsWRKY6*, the putative promoter (2000 bp upstream from ATG) was amplified from wild-type (WT) cultivar genomic DNA. The promoter amplicon was then cloned upstream of the *GUS* (*β-glucuronidase*) reporter gene in the binary vector pMDC163 using LR-based cloning. The final construct was mobilized into *Agrobacterium tumefaciens* strain (EHA105). Transgenic rice plants were produced through *Agrobacterium*-mediated transformation in scutella-derived calli,

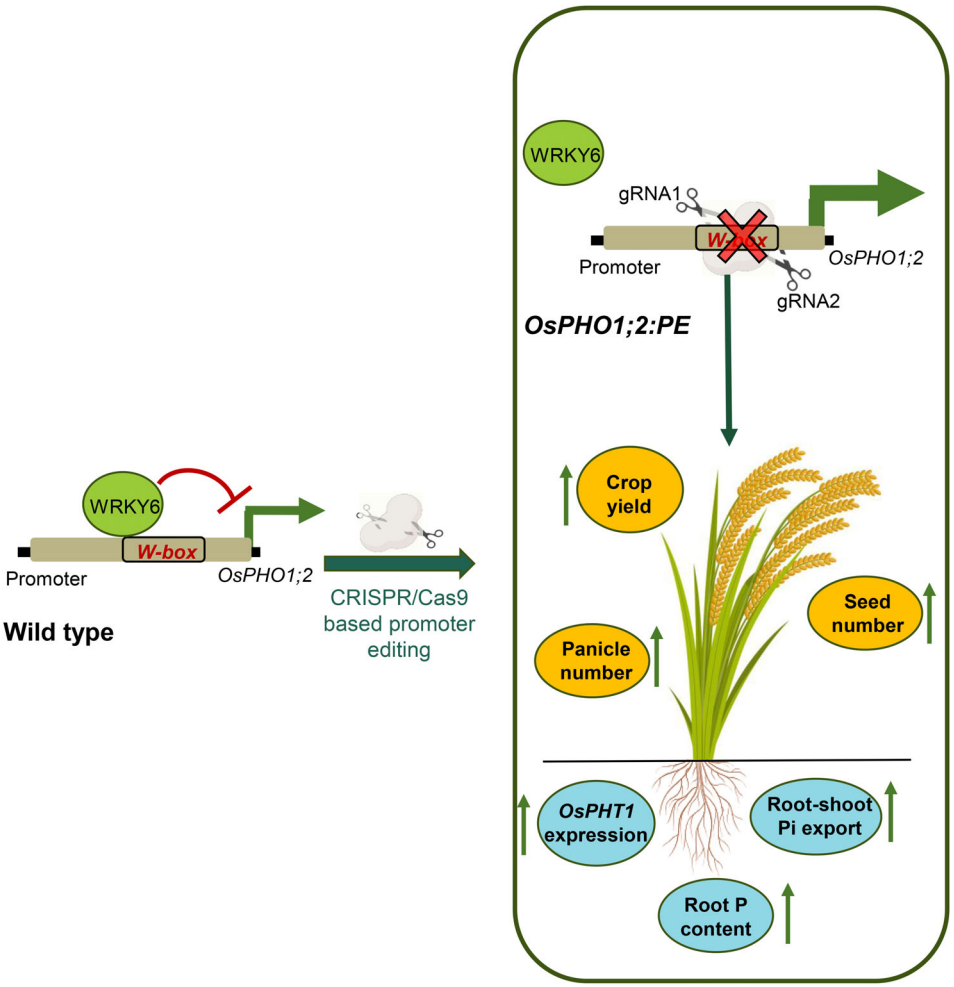

Figure 7 A proposed working model. In the WT rice, OsWRKY6 acts as a transcription repressor of *OsPHO1;2* by binding at the *W-box* site present in the *OsPHO1;2* promoter. Removal of *W-box* using CRISPR/Cas9 (*OsPHO1;2:PE*) alleviates OsWRKY6 and other potential inhibitors-mediated inhibition, thereby increasing *OsPHO1;2* expression. Such an increase in *OsPHO1;2* transcript causes more root–shoot Pi transport, high root-associated phosphate transport (*OsPHTs*) transcript level, enhanced root Pi uptake, culminating in an overall improved crop yield.

following the protocol outlined by Bhadouria *et al*. (2023). The transgenic plants were subsequently grown in a greenhouse under the previously mentioned conditions.

To generate *OsWRKY6* knockout lines, a gRNA specific to the first exon of *OsWRKY6* was designed using an online tool, CRISPR GE (http://skl.scau.edu.cn/). The designed gRNA was cloned in the destination binary vector, pRGEB32 (Xie *et al*., 2015). The final construct was used to raise transgenics, as described above. To identify CRISPR/Cas9 mutants, genomic DNA was extracted from the leaves using the Cetyltrimethylammonium bromide (CTAB) method (Murray and Thompson, 1980), and PCR amplification was performed using gene-specific primers, followed by Sanger sequencing. Positive lines were selected using the Synthego-ICE tool. The selected T2 homozygous lines were used for experimentation.

For targeting *W-box* sequence (TTGACC) present in the *OsPHO1;2* promoter, two gRNAs were designed against the nearest PAM-containing sequence spanning the *W-box* region. tRNA-gRNA complex was assembled as described (Xie *et al*., 2015). Finally, the multiplex system was cloned into a binary vector, pRGEB32. The final construct was used to raise transgenics as described above. Biallelic edited plants were then selected in the T2 generation by performing fragment-specific PCR followed by DNA sequencing. Transgene-free plants for downstream experiments were then selected after performing PCR using Cas9-specific primers (Verma *et al*., 2022). All the primers used for gRNA designing and transgenic screening are detailed in Table S4.

Analysis of off-target mutations

The CRISPR-GE tool was employed to identify potential off-targets for the gRNAs used in generating *OsPHO1;2:PE* lines. Primers were designed to amplify the potential off-target regions. The amplified PCR product was purified and sent directly for Sanger sequencing. Off-target mutations were identified using the Synthego tool (Synthego, 2019). The promoter-edited Cas9-free lines with no detectable off-target mutations were selected for further use. The primers used for screening are listed in Table S4.

Gene expression analysis

Total RNA from plant tissue was extracted using Trizol reagent (Invitrogen, Waltham, MA, USA). 1 μg RNA was reverse transcribed into cDNA using a high-capacity reverse transcription

kit (Applied Biosystems, Waltham, MA, USA). The synthesized cDNA was then used to perform real-time quantitative PCR (RT-qPCR) using SYBR® Green (Applied Biosystems, Waltham, MA, USA) master mix in the Applied Biosystems 7500 Fast Real-Time PCR instrument. Rice housekeeping gene *Ubiquitin5* was used as an endogenous control. The gene expression level was calculated using fold change ($2^{-\Delta Ct}$). Primers used in RT-qPCR are shown in Table S4.

Soluble Pi and total P content measurement

The estimation of soluble Pi in fresh tissue was performed as described by Chiou *et al*. (2006). Briefly, samples were crushed using liquid nitrogen and homogenized in an extraction buffer consisting of 10 mM Tris–HCl (pH 8.0), 1 mM EDTA, 0.1 M NaCl and 1 mM β-mercaptoethanol at a 1:10 ratio. The solution was then diluted five times in CH_3COOH and incubated for 30 min at 42 °C. Next, 300 μL of the solution was mixed with 700 μL of the assay solution (10% ascorbic acid, 0.42% ammonium molybdate in 2 N H_2SO_4), followed by another 30 min of incubation at 42 °C. The absorbance was recorded at a wavelength of 820 nm using the POLARstar Omega plate reader from BMG Labtech, Germany. Pi concentration was measured using a standard solution of 50 ppm KH_2PO_4.

The yellow vanadomolybdate method was used to measure total P in root and shoot tissues (Mehra *et al*., 2017). Briefly, the tissues were oven-dried completely at 60 °C for 3 days and then ashed at 500 °C overnight. The ash was dissolved in 2 N HCl and mixed with an ammonium metavanadate solution to form a yellow-coloured complex. Absorbance was measured at a wavelength of 410 nm in a microplate reader, using a 50 ppm KH_2PO_4 solution as the standard.

For elemental analysis (P, Fe) in seeds, brown rice powder (200 mg) was digested with 8 mL of 65% HNO_3 at 180 °C using a microwave digestion system. The samples were diluted, filtered through 0.2 μm filters and analysed with an Agilent 7800 Inductively Coupled Plasma Mass Spectrometer (ICP-MS).

Measurement of ^{33}P uptake and transport

To measure ^{33}P transfer from root to shoot, dehusked sterilized seeds of WT and *OsPHO1;2:PE* lines were germinated for 9 days in a quarter of an MS hydroponics solution. The roots of the seedlings were washed with distilled water and immersed in a ^{33}P radioactive solution (3.1 μCi/mL; 10 μM Pi) for 2 h. After incubation, the roots were washed with a 10 mM cold phosphate solution until all external radioactivity was removed. The radioactive phosphate was separately measured for the root and shoot using a scintillation counter. P transfer was then calculated by dividing the shoot radioactivity by the total radioactivity in the plants. To obtain ^{33}P uptake kinetics within the plant, the total plant radioactivity per mg of fresh weight of roots was calculated.

Root system architecture traits quantification

Seeds were pregerminated on 1/4th MS media for four days and then transferred to hydroponics in Yoshida media supplemented with low P (10 μM NaH_2PO_4, LP) and normal phosphorus (320 μM NaH_2PO_4, NP) concentrations. Roots were harvested after 21 days of treatment and fixed in FAA fixative solution consisting of 10% formaldehyde, 50% ethanol and 5% acetic acid. For measurement, roots were stained with neutral red dye (0.5 mg/mL) and then scanned using the EPSON Perfection V850 Pro scanner in professional mode. Finally, scanned images were analysed using RhizoVision Explorer v2.0.3 by applying the prescribed algorithms (Seethepalli *et al*., 2021).

Electrophoretic mobility shift assay (EMSA)

The DNA binding domain of OsWRKY6 (amino acids: 222–380) was amplified using cDNA from rice seedlings and cloned into the pMALc2x vector for fusion with the N terminal MBP tag. The WRKY-MBP fusion protein was expressed in the *E. coli* strain BL21 with induction using 0.2 mM IPTG for 12–14 h at 22 °C, followed by purification with MBP resin. The oligo duplex (30 bp) containing the WRKY binding site *W-box* element ('TTGACC') and the mutant probe ('TTGACC' was replaced by 'AAAAAA') was labelled using the DIG Oligonucleotide 3'-End Labelling Kit (Roche, Basel, Switzerland). Twenty nanograms of labelled probes were incubated for 30 min at 22 °C with 5 μg recombinant protein in the binding buffer (1 μg poly(dI-dC), 15 mM HEPES (pH 8), 1 mM $MgCl_2$, 30 mM KCl, 0.02 mM DTT, 0.2 mM EDTA and 0.6% glycerol). The reaction solution was run on a native polyacrylamide gel (4% v/v) for 3 h and then transferred to a positively charged nylon membrane, followed by UV crosslinking. Band shifts were finally detected on X-ray film using the Anti-Digoxigenin-AP, Fab fragments kit (Roche, Basel, Switzerland). Primers and probes used in the experiment are listed in Table S4.

Subcellular localization and histochemical GUS staining

The full-length coding sequence of OsWRKY6, including the stop codon, was amplified and cloned into the pSITE3cA vector to generate 35S:eYFP-OsWRKY6. This construct, along with the nuclear marker 35S:RFP-NLS, was co-transformed into *N. benthamiana* leaves using the *A. tumefaciens* (EHA 105) mediated infiltration method as described by Zhang *et al*. (2020). The fluorescence signal was observed using a confocal laser scanning microscope (Leica TCS SP5; Leica Microsystems, Wetzlar, Germany). The primers employed in the experiment are listed in Table S4.

Histochemical localization of GUS activity in *OsWRKY6p:GUS* plants was conducted as described previously (Jefferson *et al*., 1987). In brief, various tissues from *OsWRKY6p*:GUS transgenics were incubated in GUS staining buffer that contained the GUS substrate (1 mm 5-bromo-4-chloro-3-indolyl-β-d-glucuronide) at 37 °C for 2–3 days. After the colour developed, tissues were immersed overnight in 70%(v/v) ethanol to remove chlorophyll. Images of the tissues were captured using the Leica S9i light microscope, Wetzlar, Germany.

Transient expression assay

The transient expression assay was conducted on rice seedlings as described previously (Singh *et al*., 2023). In summary, approximately 1.4 kb of the putative promoter region of *OsPHO1;2*, which includes the *W-box*, was cloned into the pCAMBIA1303 vector by replacing the CaMV35S promoter upstream of the GUS gene and transformed into *Agrobacterium* (EHA 105). The cells were cultured overnight at 28 °C. Once the OD reached 0.6–0.8, the cells were harvested and resuspended in infiltration buffer (10 mM MES, 10 mM $MgCl_2$ and 100 mM acetosyringone). Three-day-old rice seedlings (WT and *oswrky6*) were incubated in the *Agrobacterium* culture and then vacuum infiltrated. The seedlings were placed in a growth chamber for 2–3 days, after which GUS activity was analysed. GUS staining of the roots was performed as described above. The primers used in the experiment are listed in Table S4.

To quantify GUS activity, the fluorometric MUG assay was performed as described by Francis and Spiker (2005). Briefly, total protein was isolated from rice roots using GUS extraction buffer (150 mM sodium phosphate at pH 7.0, 10 mM EDTA, 10 mM β-mercaptoethanol, 0.1% Triton X-100, 140 μM PMSF and 0.1% sarcosyl). Thirteen μg of isolated protein from WT and *oswrky6* roots was incubated with GUS assay buffer (GUS extraction buffer containing 1.2 mM 4-methylumbelliferyl β-D-glucuronide (MUG), Sigma) at 37 °C in the dark. After one hour of incubation, 10 μL of the reaction mix was added to 190 μL of stop buffer (200 mM sodium carbonate) in a 96-well opaque microplate. 4-MU (4-methylumbelliferone) was used as a standard. Fluorescence was measured using a POLARstar Omega plate reader with excitation at 355 nm and emission at 460 nm. GUS activity was reported as nM/min/mg protein.

Starch and amylose estimation

Dehusked rice seeds were dried and ground to estimate the total starch content. Starch estimation was conducted according to the Total Starch (AA/AMG) Assay Kit (Megazyme, Bray, Ireland), following all steps as per the manufacturer's instructions. The available total starch was calculated using the Mega-Calc™ software tool.

The iodine-potassium iodide (I_2:KI) procedure was employed to estimate amylose (Juliano, 1971). Briefly, 100 mg of crushed seeds were mixed with 20 μL of 95% ethanol and 180 μL of 1 M NaOH, then incubated in boiling water for 10 min. The volume was adjusted to 2 mL. A 100 μL aliquot of the solution was mixed with 20 μL of acetic acid and 40 μL of 0.2% I_2-KI reagent. Absorbance was subsequently recorded at 620 nm using a POLARstar Omega plate reader (BMG Labtech, Germany). The amylose content was calculated based on a standard graph (Avaro *et al*., 2011).

To observe the morphology of starch granules, dehulled seeds were crushed into a fine powder using a tissue lyser, followed by staining with Lugol solution (iodine: potassium iodine solution diluted in deionized water [1:10]; Himedia) for at least 10 s. The starch granules were then examined under a light microscope.

The packaging of starch granules was visualized using a scanning electron microscope (SEM, EVO® LS10 Zeiss, Oberkochen, Germany). Mature seeds were cut from the centre of the endosperm, and photographs were taken at a magnification of 2500×.

Phytic acid measurement

Phytic acid was measured in rice seeds using the Phytic Acid Assay Kit (Megazyme K-PHYT, Bray, Ireland) according to the manufacturer's instructions. Briefly, 200 mg of crushed seeds were placed in glass tubes, and 2 mL of 0.66 M HCl was added. The tubes were then incubated in a shaker at 28 °C and 200 rpm for 5–6 h. One mL of extraction was centrifuged at 13 000 rpm, and the supernatant (0.5 mL) was then transferred to another tube, followed by the addition of 0.75 M NaOH (0.5 mL) to neutralize it. The subsequent steps for measuring free and total phosphorus were performed as described (Megazyme K-PHYT, Bray, Ireland). The calculation for phytic acid was done using the Mega-Calc™ software tool (Megazyme K-PHYT, Bray, Ireland).

Statistical analysis

All numerical data are presented as means with standard error bars. Statistical significance was determined using pairwise Student's *t*-tests conducted with Microsoft Office Excel. Statistical significance is indicated by: * for $P \leq 0.05$, ** for $P \leq 0.01$ and *** for $P \leq 0.001$. Data from Figure 1a were analysed using Brown-Forsythe and Welch's one-way ANOVA tests, followed by multiple comparisons with *P* values ($P < 0.05$) adjusted using FDR.

Acknowledgements

This research is funded by the Indo-Swiss joint research project (BT/IN/Swiss/46/JG/2018-2019 to JG and IZLIZ3_183114/1 to YP) and a grant from the Herbette Foundation at the University of Lausanne. Research fellowships to K.M. from CSIR, India; B.M. from DBT, India; and B.S. and U.S. from NIPGR, India, are gratefully acknowledged.

Conflict of interest

The authors declare no conflicts of interest.

Author contributions

K.M. conducted most experiments, analysed data and wrote the manuscript. B.M. conducted experiments, analysed data and edited the manuscript. B.S., U.S. and A.J. helped with the experiments. S.S., R.P., H.V.T. and S.K.M. helped with soil-based experiments. J.G. and Y.P. conceived the project; J.G. supervised experiments, analysed data and finalized the manuscript with help from Y.P.

Data availability statement

All relevant data generated or analysed are included in the manuscript with supporting materials.

References

Ahmar, S., Saeed, S., Khan, M.H.U., Ullah Khan, S., Mora-Poblete, F., Kamran, M., Faheem, A. *et al*. (2020) A revolution toward gene-editing technology and its application to crop improvement. *Int. J. Mol. Sci.* **21**, 5665.

Avaro, M.R.A., Pan, Z., Yoshida, T. and Wada, Y. (2011) Two alternative methods to predict amylose content of rice grain by using tristimulus CIE lab values and developing a specific color board of starch-iodine complex solution. *Plant Prod. Sci.* **14**, 164–168.

Bhadouria, J., Mehra, P., Verma, L., Pazhamala, L.T., Rumi, R., Panchal, P., Sinha, A.K. *et al*. (2023) Root-expressed rice PAP3b enhances secreted APase activity and helps utilize organic phosphate. *Plant Cell Physiol.* **64**, 501–518.

Bloot, A.P.M., Kalschne, D.L., Amaral, J.A.S., Baraldi, I.J. and Canan, C. (2021) A review of phytic acid sources, obtention, and applications. *Food Rev. Intl.* **39**, 73–92.

Brázda, V., Bartas, M. and Bowater, R.P. (2021) Evolution of diverse strategies for promoter regulation. *Trends Genet.* **37**, 730–744.

Campos-Soriano, L., Bundó, M., Bach-Pages, M., Chiang, S.-F., Chiou, T.-J. and San Segundo, B. (2020) Phosphate excess increases susceptibility to pathogen infection in rice. *Mol. Plant Pathol.* **21**, 555–570.

Che, J., Yamaji, N., Miyaji, T., Mitani-Ueno, N., Kato, Y., Shen, R.F. and Ma, J.F. (2020) Node-localized transporters of phosphorus essential for seed development in rice. *Plant Cell Physiol.* **61**, 1387–1398.

Chen, Y.-F., Li, L.-Q., Xu, Q., Kong, Y.-H., Wang, H. and Wu, W.-H. (2009) The WRKY6 transcription factor modulates PHOSPHATE1 expression in response to low Pi stress in Arabidopsis. *Plant Cell* **21**, 3554–3566.

Chiou, T.-J., Aung, K., Lin, S.-I., Wu, C.-C., Chiang, S.-F. and Su, C. (2006) Regulation of phosphate homeostasis by MicroRNA in Arabidopsis. *Plant Cell* **18**, 412–421.

Choi, C., Hwang, S., Fang, I.R., Kwon, S.I., Park, S.R., Ahn, I., Kim, J.B. *et al*. (2015) Molecular characterization of *Oryza sativa* WRKY 6, which binds to W-

box-like element 1 of the *Oryza sativa* pathogenesis-related (PR) 10a promoter and confers reduced susceptibility to pathogens. *New Phytol.* **208**, 846–859.

Dergilev, A.I., Orlova, N.G., Dobrovolskaya, O.B. and Orlov, Y.L. (2021) Statistical estimates of multiple transcription factors binding in the model plant genomes based on ChIP-seq data. *J. Integr. Bioinform.* **19**, 20200036.

Devaiah, B.N., Karthikeyan, A.S. and Raghothama, K.G. (2007) WRKY75 transcription factor is a modulator of phosphate acquisition and root development in Arabidopsis. *Plant Physiol.* **143**, 1789–1801.

Elser, J.J., Chan, N.I., Corman, J.R. and Stoltzfus, J. (2017) Save the P (ee)!: The challenges of phosphorus sustainability and emerging solutions. In *Dietary phosphorus*, pp. 327–340. Florida: CRC Press.

Francis, K.E. and Spiker, S. (2005) Identification of *Arabidopsis thaliana* transformants without selection reveals a high occurrence of silenced T-DNA integrations. *Plant J.* **41**, 464–477.

Gamuyao, R., Chin, J.H., Pariasca-Tanaka, J., Pesaresi, P., Catausan, S., Dalid, C., Slamet-Loedin, I. *et al*. (2012) The protein kinase Pstol1 from traditional rice confers tolerance of phosphorus deficiency. *Nature* **488**, 535–539.

Gu, M., Chen, A., Sun, S. and Xu, G. (2016) Complex regulation of plant phosphate transporters and the gap between molecular mechanisms and practical application: what is missing? *Mol. Plant* **9**, 396–416.

Hori, K. and Sun, J. (2022) Rice grain size and quality. *Rice* **15**, 33.

Jefferson, R.A., Kavanagh, T.A. and Bevan, M.W. (1987) GUS fusions: beta-glucuronidase as a sensitive and versatile gene fusion marker in higher plants. *EMBO J.* **6**, 3901–3907.

Jia, H., Ren, H., Gu, M., Zhao, J., Sun, S., Zhang, X. *et al*. (2011) The phosphate transporter gene OsPht1;8; is involved in phosphate homeostasis in rice. *Plant Physiol.* **156**, 1164–1175.

Jiang, H., Shi, Y., Liu, J., Li, Z., Fu, D., Wu, S., Li, M. *et al*. (2022) Natural polymorphism of ZmICE1 contributes to amino acid metabolism that impacts cold tolerance in maize. *Nat Plants* **8**, 1176–1190.

Jiang, J., Ma, S., Ye, N., Jiang, M., Cao, J. and Zhang, J. (2017) WRKY transcription factors in plant responses to stresses. *J. Integr. Plant Biol.* **59**, 86–101.

Jiao, W., Chen, W., Chang, A.C. and Page, A.L. (2012) Environmental risks of trace elements associated with long-term phosphate fertilizers applications: a review. *Environ. Pollut.* **168**, 44–53.

Juliano, B.O. (1971) A simplified assay for milled-rice amylose. *Cereal Sci. Today* **12**, 334–360.

Ko, S.-S., Lu, W.-C., Hung, J.-C., Chang, H.-F., Li, M.-J., Yeh, K.-C. and Chiou, T.-J. (2024) Maternal effect contributes to grain-filling defects of Ospho1;2 rice mutants. *New Phytol.* **244**, 351–357.

Langhans, C., Beusen, A.H.W., Mogollón, J.M. and Bouwman, A.F. (2022) Phosphorus for sustainable development goal target of doubling smallholder productivity. *Nat Sustain* **5**, 57–63.

Lay-Pruitt, K.S., Wang, W., Prom-U-Thai, C., Pandey, A., Zheng, L. and Rouached, H. (2022) A tale of two players: the role of phosphate in iron and zinc homeostatic interactions. *Planta* **256**, 23.

Lescot, M., Déhais, P., Thijs, G., Marchal, K., Moreau, Y., Van de Peer, Y. *et al*. (2002) PlantCARE, a database of plant cis-acting regulatory elements and a portal to tools for in silico analysis of promoter sequences. *Nucleic Acids Res.* **30**, 325–327.

Liu, F., Wang, Z., Ren, H., Shen, C., Li, Y., Ling, H.-Q., Wu, C. *et al*. (2010) OsSPX1 suppresses the function of OsPHR2 in the regulation of expression of OsPT2 and phosphate homeostasis in shoots of rice. *Plant J.* **62**, 508–517.

López-Arredondo, D.L. and Herrera-Estrella, L. (2012) Engineering phosphorus metabolism in plants to produce a dual fertilization and weed control system. *Nat. Biotechnol.* **30**, 889–893.

López-Arredondo, D.L., Leyva-González, M.A., González-Morales, S.I., López-Bucio, J. and Herrera-Estrella, L. (2014) Phosphate nutrition: improving low-phosphate tolerance in crops. *Annu. Rev. Plant Biol.* **65**, 95–123.

Lun, F., Liu, J., Ciais, P., Nesme, T., Chang, J., Wang, R., Goll, D. *et al*. (2018) Global and regional phosphorus budgets in agricultural systems and their implications for phosphorus-use efficiency. *Earth Syst Sci Data* **10**, 1–18.

Luo, B., Sahito, J. H., Zhang, H., Zhao, J., Yang, G., Wang, W., *et al*. (2024). SPX family response to low phosphorus stress and the involvement of ZmSPX1 in phosphorus homeostasis in maize. *Front. Plant Sci.*, **15**, 1385977.

Ma, B., Zhang, L., Gao, Q., Wang, J., Li, X., Wang, H., Liu, Y. *et al*. (2021) A plasma membrane transporter coordinates phosphate reallocation and grain filling in cereals. *Nat. Genet.* **53**, 906–915.

Ma, B., Zhang, Y., Fan, Y., Zhang, L., Li, X., Zhang, Q.-Q., Shu, Q. *et al*. (2024) Genetic improvement of phosphate-limited photosynthesis for high yield in rice. *Proc. Natl. Acad. Sci.* **121**, e2404199121.

MacDonald, G.K., Bennett, E.M., Potter, P.A. and Ramankutty, N. (2011) Agronomic phosphorus imbalances across the world's croplands. *Proc. Natl. Acad. Sci.* **108**, 3086–3091.

Mani, B., Maurya, K., Kohli, P.S. and Giri, J. (2024) Chickpea (*Cicer arietinum*) PHO1 family members function redundantly in Pi transport and root nodulation. *Plant Physiol. Biochem.* **211**, 108712.

McDowell, R.W., Pletnyakov, P. and Haygarth, P.M. (2024) Phosphorus applications adjusted to optimal crop yields can help sustain global phosphorus reserves. *Nat Food* **5**, 332–339.

Mehra, P., Pandey, B.K. and Giri, J. (2017) Improvement in phosphate acquisition and utilization by a secretory purple acid phosphatase (OsPAP21b) in rice. *Plant Biotechnol. J.* **15**, 1054–1067.

Mehra, P., Pandey, B.K., Verma, L. and Giri, J. (2019) A novel glycerophosphodiester phosphodiesterase improves phosphate deficiency tolerance in rice. *Plant Cell Environ.* **42**, 1167–1179.

Mudge, S.R., Rae, A.L., Diatloff, E. and Smith, F.W. (2002) Expression analysis suggests novel roles for members of the Pht1 family of phosphate transporters in Arabidopsis. *Plant J.* **31**, 341–353.

Murray, M.G. and Thompson, W. (1980) Rapid isolation of high molecular weight plant DNA. *Nucleic Acids Res.* **8**, 4321–4326.

Nagpal, L., He, S., Rao, F. and Snyder, S.H. (2024) Inositol pyrophosphates as versatile metabolic messengers. *Annu. Rev. Biochem.* **93**, 317–338.

Navea, I.P., Yang, S., Tolangi, P., Sumabat, R.M., Zhang, W. and Chin, J.H. (2024) Enhancement of rice traits for the maintenance of the phosphorus balance between rice plants and the soil. *Curr Plant Biol* **38**, 100332.

Nissar, J., Ahad, T., Naik, H.R. and Hussain, S.Z. (2017) A review phytic acid: As antinutrient or nutraceutical. *J. Pharmacogn. Phytochem.* **6**, 1554–1560.

Nussaume, L., Kanno, S., Javot, H., Marin, E., Pochon, N., Ayadi, A., Nakanishi, T.M. *et al*. (2011) Phosphate import in plants: focus on the PHT1 transporters. *Front. Plant Sci.* **2**, 83.

Ojeda-Rivera, J.O., Alejo-Jacuinde, G., Nájera-González, H.-R. and López-Arredondo, D. (2022) Prospects of genetics and breeding for low-phosphate tolerance: an integrated approach from soil to cell. *Theor. Appl. Genet.* **135**, 4125–4150.

Paszkowski, U., Kroken, S., Roux, C., and Briggs, S. P. (2002). Rice phosphate transporters include an evolutionarily divergent gene specifically activated in arbuscular mycorrhizal symbiosis. *Proc. Natl. Acad. Sci.* , **99**, 13324–13329.

Poirier, Y., Jaskolowski, A. and Clúa, J. (2022) Phosphate acquisition and metabolism in plants. *Curr. Biol.* **32**, R623–R629.

Poirier, Y., Thoma, S., Somerville, C. and Schiefelbein, J. (1991) A mutant of Arabidopsis deficient in xylem loading of phosphate. *Plant Physiol.* **97**, 1087–1093.

Rouached, H., Stefanovic, A., Secco, D., Bulak Arpat, A., Gout, E., Bligny, R. and Poirier, Y. (2011) Uncoupling phosphate deficiency from its major effects on growth and transcriptome via PHO1 expression in Arabidopsis. *Plant J.* **65**, 557–570.

Rushton, P.J., Somssich, I.E., Ringler, P. and Shen, Q.J. (2010) WRKY transcription factors. *Trends Plant Sci.* **15**, 247–258.

Secco, D., Baumann, A. and Poirier, Y. (2010) Characterization of the rice PHO1 gene family reveals a key role for OsPHO1;2 in phosphate homeostasis and the evolution of a distinct clade in dicotyledons. *Plant Physiol.* **152**, 1693–1704.

Seethepalli, A., Dhakal, K., Griffiths, M., Guo, H., Freschet, G.T. and York, L.M. (2021) RhizoVision Explorer: open-source software for root image analysis and measurement standardization. *AoB Plants* **13**, plab056.

Shi, L., Su, J., Cho, M.-J., Song, H., Dong, X., Liang, Y. and Zhang, Z. (2023) Promoter editing for the genetic improvement of crops. *J. Exp. Bot.* **74**, 4349–4366.

Shin, D., Lee, S., Kim, T.-H., Lee, J.-H., Park, J., Lee, J., Lee, J.Y. *et al*. (2020) Natural variations at the Stay-Green gene promoter control lifespan and yield in rice cultivars. *Nat. Commun.* **11**, 2819.

Singh, A.P., Pandey, B.K., Deveshwar, P., Narnoliya, L., Parida, S.K. and Giri, J. (2015) JAZ repressors: potential involvement in nutrients deficiency response in rice and chickpea. *Front. Plant Sci.* **6**, 975.

Singh, D., Banerjee, G., Verma, N. and Sinha, A.K. (2023) MAP kinases may mediate regulation of the cell cycle in rice by E2F2 phosphorylation. *FEBS Lett.* **597**, 2993–3009.

Stefanovic, A., Ribot, C., Rouached, H., Wang, Y., Chong, J., Belbahri, L., Delessert, S. *et al*. (2007) Members of the PHO1 gene family show limited functional redundancy in phosphate transfer to the shoot, and are regulated by phosphate deficiency via distinct pathways. *Plant J.* **50**, 982–994.

Su, T., Xu, Q., Zhang, F.-C., Chen, Y., Li, L.-Q., Wu, W.-H. and Chen, Y.-F. (2015) WRKY42 modulates phosphate homeostasis through regulating phosphate translocation and acquisition in Arabidopsis. *Plant Physiol.* **167**, 1579–1591.

Synthego. (2019) *Synthego Performance Analysis, ICE Analysis. v3.0*.

Tang, X. and Zhang, Y. (2023) Beyond knockouts: fine-tuning regulation of gene expression in plants with CRISPR-Cas-based promoter editing. *New Phytol.* **239**, 868–874.

Ulker, B. and Somssich, I.E. (2004) WRKY transcription factors: from DNA binding towards biological function. *Curr. Opin. Plant Biol.* **7**, 491–498.

Venezia, M. and Creasey Krainer, K.M. (2021) Current advancements and limitations of gene editing in orphan crops. *Front. Plant Sci.* **12**, 742932.

Verma, L., Bhadouria, J., Bhunia, R.K., Singh, S., Panchal, P., Bhatia, C., Eastmond, P.J. *et al*. (2022) Monogalactosyl diacylglycerol synthase 3 affects phosphate utilization and acquisition in rice. *J. Exp. Bot.* **73**, 5033–5051.

Wang, H., Cheng, X., Yin, D., Chen, D., Luo, C., Liu, H. and Huang, C. (2023) Advances in the research on plant WRKY transcription factors responsive to external stresses. *Curr. Issues Mol. Biol.* **45**, 2861–2880.

Wang, L., O'Conner, S., Tanvir, R., Zheng, W., Cothron, S., Towery, K. *et al*. (2024) CRISPR/Cas9-based editing of NF-YC4 promoters yields high-protein rice and soybean. *New Phytol.* **245**, 2103–2116.

Wang, X., Wang, Y., Piñeros, M.A., Wang, Z., Wang, W., Li, C., Wu, Z. *et al*. (2014) Phosphate transporters OsPHT1;9 and OsPHT1;10 are involved in phosphate uptake in rice. *Plant Cell Environ.* **37**, 1159–1170.

Wang, Y., Ribot, C., Rezzonico, E. and Poirier, Y. (2004) Structure and expression profile of the Arabidopsis PHO1 gene family indicates a broad role in inorganic phosphate homeostasis. *Plant Physiol.* **135**, 400–411.

Wang, Z., Kuo, H.-F. and Chiou, T.-J. (2021) Intracellular phosphate sensing and regulation of phosphate transport systems in plants. *Plant Physiol.* **187**, 2043–2055.

Wani, S.H., Anand, S., Singh, B., Bohra, A. and Joshi, R. (2021) WRKY transcription factors and plant defense responses: latest discoveries and future prospects. *Plant Cell Rep.* **40**, 1071–1085.

Wege, S., Khan, G.A., Jung, J.Y., Vogiatzaki, E., Pradervand, S., Aller, I. *et al*. (2016) The EXS Domain of PHO1 participates in the response of shoots to phosphate deficiency via a root-to-shoot signal1[OPEN]. *Plant Physiol.* **170**, 385–400.

Wu, B., Luo, H., Chen, Z., Amin, B., Yang, M., Li, Z., Wu, S. *et al*. (2024) Rice promoter editing: an efficient genetic improvement strategy. *Rice* **17**, 55.

Wu, K.-L., Guo, Z.-J., Wang, H.-H. and Li, J. (2005) The WRKY family of transcription factors in rice and Arabidopsis and their origins. *DNA Res.* **12**, 9–26.

Wu, W.-S. and Lai, F.-J. (2015) Functional redundancy of transcription factors explains why most binding targets of a transcription factor are not affected when the transcription factor is knocked out. *BMC Syst. Biol.* **9**, S2.

Xie, K., Minkenberg, B. and Yang, Y. (2015) Boosting CRISPR/Cas9 multiplex editing capability with the endogenous tRNA-processing system. *Proc. Natl. Acad. Sci.* **112**, 3570–3575.

Yang, S.-Y., Lin, W.-Y., Hsiao, Y.-M. and Chiou, T.-J. (2024) Milestones in understanding transport, sensing, and signaling of the plant nutrient phosphorus. *Plant Cell* **36**, 1504–1523.

Ye, Q., Wang, H., Su, T., Wu, W.H. and Chen, Y.F. (2018) The ubiquitin E3 ligase PRU1 regulates WRKY6 degradation to modulate phosphate homeostasis in response to low-Pi stress in Arabidopsis. *Plant Cell* **30**, 1062–1076.

Yu, S., Ma, Y. and Sun, D.-W. (2009) Impact of amylose content on starch retrogradation and texture of cooked milled rice during storage. *J Cereal Sci* **50**, 139–144.

Zhang, F., Wu, X.-N., Zhou, H.-M., Wang, D.-F., Jiang, T.-T., Sun, Y.-F., Cao, Y. *et al*. (2014) Overexpression of rice phosphate transporter gene OsPT6 enhances phosphate uptake and accumulation in transgenic rice plants. *Plant and Soil* **384**, 259–270.

Zhang, Y., Chen, M., Siemiatkowska, B., Toleco, M.R., Jing, Y., Strotmann, V., Zhang, J. *et al*. (2020) A highly efficient agrobacterium-mediated method for transient gene expression and functional studies in multiple plant species. *Plant Commun* **1**, 100028.

Zhao, P., You, Q. and Lei, M. (2019) A CRISPR/Cas9 deletion into the phosphate transporter SlPHO1; 1 reveals its role in phosphate nutrition of tomato seedlings. *Physiol. Plant.* **167**, 556–563.

Zhou, H., Xia, D. and He, Y. (2020) Rice grain quality—traditional traits for high quality rice and health-plus substances. *Mol. Breed.* **40**, 1–17.

Zhou, J., Liu, G., Zhao, Y., Zhang, R., Tang, X., Li, L., Jia, X. *et al*. (2023) An efficient CRISPR–Cas12a promoter editing system for crop improvement. *Nat Plants* **9**, 588–604.

Zhu, D., Li, M., Fang, C., Yu, J., Zhu, Z., Yu, Y. and Shao, Y. (2023) Effects of storage on the starch fine structure and physicochemical properties of different rice variety types. *Carbohydr. Polym.* **300**, 120273.

Zou, T., Zhang, X. and Davidson, E.A. (2022) Global trends of cropland phosphorus use and sustainability challenges. *Nature* **611**, 81–87.

Supporting information

Additional supporting information may be found online in the Supporting Information section at the end of the article.

Figure S1 Subcellular location of OsWRKY6 in *N. benthamiana* leaves.

Figure S2 Generation of os*wrky6* knockout mutants using CRISPR/Cas9.

Figure S3 *OsWRKY6* expression levels in *oswrky6* knockout mutants.

Figure S4 GUS expression in cross-section of wild type (WT) and *oswrky6* roots.

Figure S5 Phenotypic analysis of os*wrky6* knockouts.

Figure S6 Genotypic analysis of *OsPHO1;2:PE* plants.

Figure S7 Cas9 detection in T2 generation of *OsPHO1;2:PE* marker-free lines.

Figure S8 Total shoot P concentration and shoot dry biomass in WT and *OsPHO1;2:PE* lines.

Figure S9 Total root P concentration and root efficiency in WT and *OsPHO1;2:PE* lines.

Figure S10 Evaluation of agronomic traits in WT and *OsPHO1;2:PE* lines (Year 2023).

Figure S11 Evaluation of agronomic traits in WT and *OsPHO1;2:PE* lines (Year 2024).

Figure S12 Evaluation of agronomic traits in WT and *OsPHO1;2:PE* lines under low P fertilizer supply.

Figure S13 Amylose content quantification and starch granule visualization in seeds of WT and *OsPHO1;2:PE* lines.

Figure S14 Evaluation of grain physiological P use efficiency (PPUE) in WT and *OsPHO1;2:PE* lines.

Figure S15 *OsPHO1;2:PE* lines show no alteration in seed Fe content.

Table S1 Genes co-expressing with *OsPHO1;2*.

Table S2 Putative CRISPR/Cas9 off-targets for gRNAs used in the generation of *OSPHO1;2:PE* lines.

Table S3 Off-targets (OT) prediction for gRNAs used in the generation of *OsPHO1;2:PE* lines.

Table S4 List of the primers and probes used in this study.